ACS OMEGA

Open Access

http://pubs.acs.org/journal/acsodf

Article

Instantaneous Hydrolysis of Methyl Paraoxon Nerve Agent Simulant Is Catalyzed by Nontoxic Aminoguanidine Imines

Emmanuel Kingsley Darkwah, Puspa Aryal, Chi Zhang, Charles B. Musgrave, III, William A. Goddard, III,* and V. Prakash Reddy*

Cite This: *ACS Omega* 2025, 10, 12294−12305

Read Online

ACCESS | Metrics & More | Article Recommendations | Supporting Information

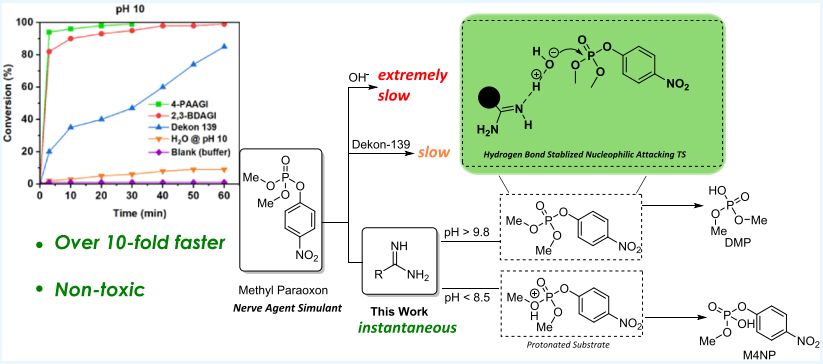

ABSTRACT: Exposure to organophosphate-based nerve agents and pesticides poses health and security threats to civilians, soldiers, and first responders. Thus, there is a need to develop effective decontamination agents that are nonhazardous to human health. To address this, we demonstrate that instantaneous hydrolysis of methyl paraoxon (Me-POX), a nerve agent simulant, can be achieved in the presence of aminoguanidine imines at pH 10: ● the pyridine-4-aldehyde aminoguanidine-imine (**1**) and ● the 2,3-butanedione aminoguanidine-imine (**2**). The hydrolysis of Me-POX under these conditions is substantially faster than that of the state-of-the-art decontaminating agent, Dekon-139 (2,3-butanedione oxime, potassium salt). Furthermore, Dekon-139 shows adverse effects when applied on skin surfaces, making it of great interest to develop safer but effective decontaminating agents for neutralizing nerve agents and pesticides exposed to skin-surface areas. Our pharmaceutically relevant aminoguanidine derivatives serve as rather nontoxic and safe decontaminating agents for organophosphate-based nerve agents and pesticides. The hydrolytic degradation products of Me-POX by our aminoguanidine-based imines and Dekon-139 are pH dependent. At pH > 10, Me-POX is hydrolyzed to give dimethyl phosphate as the exclusive product, whereas at pH < 9, the major product of hydrolysis is methyl 4-nitrophenyl phosphate (M4NP). We applied Quantum Mechanics calculations to investigate the mechanism of this dramatically accelerated decontamination process. We predict that in the rate-determining transition state, both **1** and **2** stabilize the reaction center through hydrogen bonding. Compared to Dekon-139, the rate constants of the rate-determine steps (RDS) are predicted to be over 9,000 times larger for **1** and over 600 times larger for **2**, explaining the improvement. Quantum Mechanics calculations rationalize the pH-dependent hydrolysis products of the Me-POX in the gas phase, and gauge-including atomic orbital (GIAO)-^{31}P NMR chemical shift calculations confirm the experimental values.

INTRODUCTION

In spite of the international treaties banning the use and production of nerve agents, they continue to pose dangerous health and security threats to civilians, soldiers, and first respondents, as exemplified by the recent terrorist attacks using these prohibited chemical warfare agents (CWAs).[1,2] Almost all of the nerve agents are organophosphate-derived compounds, which are highly reactive because the acyl nucleophilic substitutions (SN_2(Ac)) in the hydrolytic breakdown of these compounds are accelerated by the high electrophilicity of the phosphonyl moiety and super leaving groups, such as fluoride ion in case of nerve agents GB (isopropyl methylfluorophosphonate; Sarin), GF (cyclohexyl methylfluorophosphonate; cyclosarin), GV [2-(dimethylamino)ethyl *N*,*N*-dimethylphosphoramidofluoridate], and GD (pinacolyl methylfluorophosphonate; Soman) (Figure 1A).[3]

Received: December 11, 2024
Revised: February 11, 2025
Accepted: February 14, 2025
Published: March 21, 2025

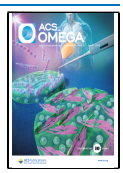

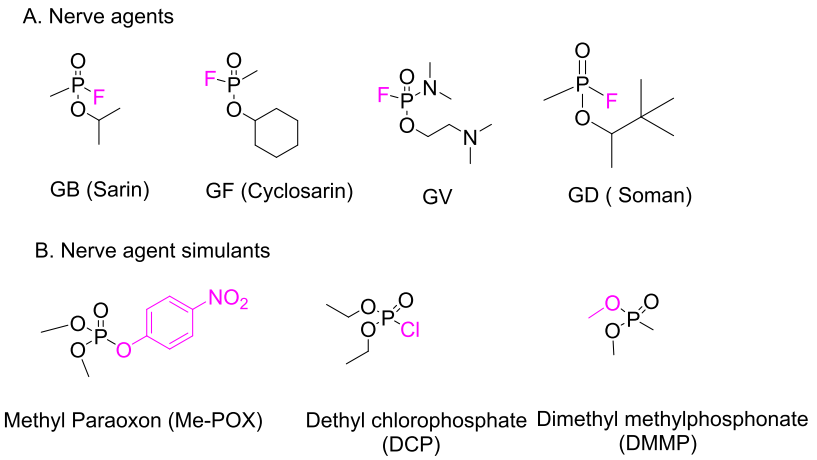

Figure 1. Structures of some organophosphate-based nerve agents (GB, GF, GV, and GD) and nerve agent simulants (Me-POX, DCP, DMMP).

Organophosphate-based pesticides and analogs, such as methyl paraoxon (Me-POX), diethyl chlorophosphate (DCP), and dimethyl methylphosphonate (DMMP), have structural similarities to the nerve agents but are substantially less toxic than the nerve agents (Figure 1B). These latter organophosphate-derived simulants are widely used in the detoxification (decontamination) studies of the nerve agents.

Organophosphate-derived nerve agents bind irreversibly to the active site serine residues of acetyl cholinesterase (AChE), as well as to butyryl cholinesterase and carboxyesterase, thereby irreversibly inactivating the enzymes.[4] This irreversible inactivation of the AChE results in the excessive and persistent accumulation of the neurotransmitter acetylcholine at the neuronal synapses resulting in permanent disability to the affected individuals.[5] Recent research efforts focused on developing and designing reactive and cost-effective materials aimed at degrading chemical warfare agents (CWAs)[6,7] have investigated such materials as heterogeneous catalysts,[8] titanium-based nanomaterials,[9] metal−organic frameworks (MOFs),[10,11] enzymes,[12] reactive polymers,[13,14] coatings and sensors,[15] smart fabrics,[16,17] and compounds featuring carboxyl (−COOH) and amino groups ($-NH_2$) with side-chain groups (R: alkyl/aryl)—categorized as soft and hard bases in nucleophilic catalysis.[18] In particular, MOFs have emerged as highly effective, versatile, and customizable materials for the catalytic degradation of nerve agents and their simulants. Notably, Zirconium (Zr)-based MOFs such as UiO-66, NU-1000, and MOF-808 have been particularly effective in breaking down these hazardous compounds.[19−22] For instance, Farha[23] and others[24,25] have engineered a variety of Zr-based MOFs with diverse chemical functionalities for the catalytic hydrolysis of nerve agent simulants like Me-POX, diisopropyl fluorophosphate (DFP), as well as nerve agents tabun, sarin, soman, and *O*-ethyl *S*-[2-(diisopropylamino)ethyl] methylphosphono-thioate (VX).[26] Current research also highlights the potential applications of MOFs in drug delivery systems, including the encapsulation and controlled release of pharmaceuticals, leveraging their porous structures to accommodate and safeguard active ingredients. However, challenges such as biocompatibility, stability in physiological conditions, and scalability for industrial production currently limit their widespread use in medicinal products.[27] Thus, the application of MOFs in medicinal product formulations is still being explored and is not widely established.

There is an emerging interest in developing pharmaceuticals and skin-decontaminating agents that counteract the acute and long-term toxicity effects of nerve agents. Currently, there is only one FDA-approved skin-decontaminating agent, Reactive Skin Decontaminating Lotion (RSDL), for nerve agent and pesticide decontamination.[28−30] The active ingredient of RSDL, the potassium salt of 2,3-Butanedione monooxime (Dekon-139), is used as a topical decontaminating agent at pH > 10, even though it exhibits adverse effects upon its topical administration, including paralysis of skeletal muscles[31,32] and impaired wound healing when applied to the open wounds.[33] Intravenous injections of this decontaminating agent result in systemic toxicity, whereas topical administration results in relatively less severe toxicity. Based on this evidence, FDA has recommended not to "use RSDL for whole body decontamination or use excessive quantities."[34]

In order to create safer and effective surface decontaminating agents for the degradation of organophosphate nerve agents and pesticides, we demonstrate here the instantaneous hydrolysis of methyl paraoxon, a nerve agent simulant, in the presence of pharmaceutically relevant aminoguanidine-derived aldimines: pyridine-4-aldehyde aminoguanidine-imine (**1**, 4-PAAGI) and 2,3-butanedione aminoguanidine-imine (**2**, 2,3-BDAGI) at pH 10. The rate of hydrolysis of methyl paraoxon in the presence of these catalysts is substantially higher than that in the presence of the Dekon-139 (**3**), at pH 8.5−10, making them more effective and safer.

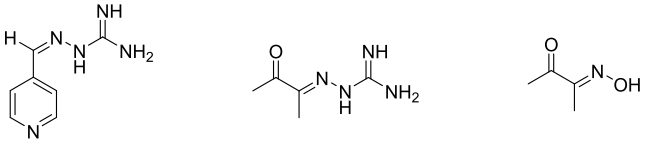

RESULTS AND DISCUSSION

Toward developing a safer and effective nerve agent and pesticide decontaminating agents, we designed and synthesized aminoguanidine imines **1** and **2** and investigated their relative rates of hydrolysis of a nerve agent simulant, methyl paraoxon (Me-POX). We compare these to the FDA-approved state-of-the-art decontaminating agent Dekon-139 (compound **3**; used as its potassium salt for skin-surface decontamination).

https://doi.org/10.1021/acsomega.4c09946
ACS Omega 2025, 10, 12294−12305

Dekon-139 has adverse effects when administered on the skin surfaces that limits its applications as a decontaminating agent.[31,32] There have been various clinical trials of aminoguanidine (pimagedine) as a drug candidate to treat diabetes and atherosclerosis,[35−40] showing that unlike the Dekon-139, aminoguanidine derivatives **1** and **2** have favorable safety profiles when administered as drug candidates or as surface decontaminating agents. Thus, compounds **1** and **2** would provide a relatively nontoxic and effective surface decontaminating agent compared to Dekon-139, the only FDA-approved skin-surface decontaminating agent.

We have synthesized new pesticide/nerve agent decontaminating agents **1** and **2** from the corresponding carbonyl compounds and aminoguanidine (see Schemes S2 and S3) under mildly acidic conditions.[41−43] Dekon-139 (**3**) was similarly synthesized from the reaction of the 2,3-butanedione with hydroxylamine hydrochloride[44,45] (Scheme S3). In glycine buffer medium at pH 10, under ambient conditions, the aminoguanidine-derived aldimines **1** and **2** hydrolyzed Me-POX (δ^{31}P = −4.9) nearly instantaneously (<3 min; the time required to acquire the ^{31}P NMR) to give dimethyl phosphate (DMP; δ^{31}P = 2.2). In contrast, under these conditions, in the presence of Dekon-139 (**3**), the hydrolysis proceeded only to the extent of 20% (Figure 2). Under otherwise similar reaction conditions (i.e., in glycine buffer medium at pH 10), in the absence of any catalyst, Me-POX remained intact, even after over 10 h. Under these conditions, after 72 h, Me-POX hydrolyzed to give M4NP to the extent of 35% (Figure S24). These results show that even at pH 10, catalysts **1**, **2**, and **3** are required for the hydrolysis of Me-POX. Interestingly, in the absence of any catalyst, Me-POX gives M4NP as the product, whereas in the presence of catalysts **1**, **2**, and **3**, DMP is formed as the exclusive product at pH 10, indicating the lack of free hydroxide anion species in the buffer media even at high pH (Figures 2, 3, and 4).

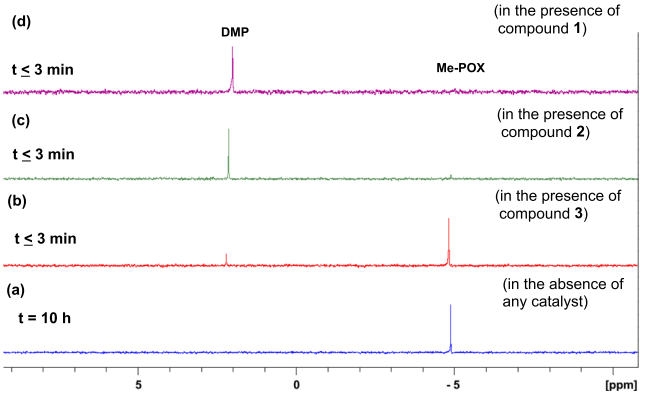

Figure 2. Proton-decoupled ^{31}P NMR spectra (161.9 MHz) for the reaction of Me-POX with small-molecule decontaminating agents.

- in 1.0 M glycine buffer (in DMSO); pH 9.8 at 25 °C, in the absence of any decontaminating agents (a);
- in the presence of
  - Dekon-139 (**3**) (b),
  - 2,3-butanedione aminoguanidine imine (**2**) (c), and
  - 4-pyridine carboxaldehyde aminoguanidine imine (**1**) (d),

under the same reaction conditions, in 3 min of reaction time.

Me-POX (δ^{31}P = −4.9) was hydrolyzed almost quantitatively to DMP (δ^{31}P = 2.2) in the presence of the 4-pyridine carboxaldehyde aminoguanidine imine (**1**) and 2,3-butanedione aminoguanidine imine (**2**), whereas in the presence of Dekon-139 (**3**), the hydrolysis of Me-POX proceeded only to the extent of 20%.

We have observed that in borate as well as in the glycine buffer media, the hydrolysis products of the Me-POX are pH dependent:

- at relatively high pH (pH > 10), dimethyl phosphate (DMP; δ^{13}P = 2.2, septet, $^{3}J_{P-H}$ = 11 Hz) is the only observed product (Scheme 1, Figures 4, 5, 6, and 7).
- at relatively low pH (pH ≤ 9), the reaction proceeds at somewhat slower rates to give M4NP as the major product (δ^{13}P = −5.5, q, $^{3}J_{P-H}$ = 11 Hz) (Scheme 1, Figures 4 and 8).
- At pH < 8.5, after 60 min of reaction time, the hydrolysis of Me-POX was complete to the extent of 48, 42, and 25%, in the presence of catalysts **1**, **2**, and **3** (Dekon-139), respectively (Figure 5c).
- Under otherwise similar conditions (pH 9.8), in the absence of the catalysts **1**, **2**, and **3**, Me-POX remained intact (i.e., 0% conversion) even after 10 h (Figure 2).

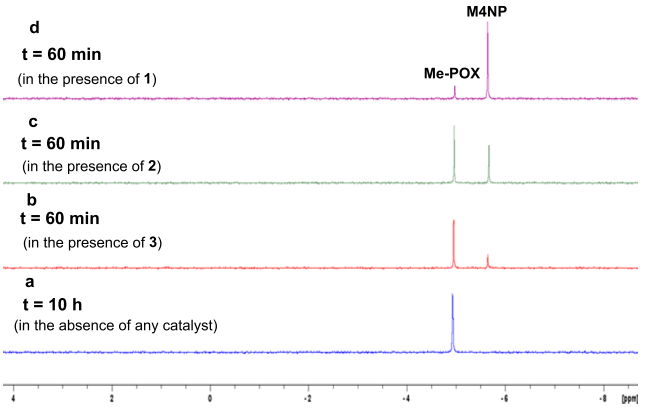

Figure 3. Proton-decoupled ^{31}P NMR spectra (161.9 MHz) for the reaction of Me-POX with small-molecule decontaminating agents in 0.5 M borate buffer (in DMSO); pH 8.5 at 25 °C.

- in the absence of any decontaminating agents (a); and
- in the presence of Dekon-139 (**3**) (b),
- 2,3-butanedione aminoguanidine imine (**2**) (c), and
- Pyridine-4- carboxaldehyde aminoguanidine imine (**1**) (d),

under the same reaction conditions in 60 min of reaction time.

- at pH < 8.5, the hydrolytic degradation of Me-POX is substantially slower and methyl 4-nitrophenyl phosphate (M4NP) is formed as the predominant product (δ^{31}P −5.5).
- In the absence of any catalyst Me-POX remained intact even after 10 h (Figures 2 and 3).

https://doi.org/10.1021/acsomega.4c09946
ACS Omega 2025, 10, 12294−12305

Scheme 1. pH-Dependent Hydrolytic Products of Methyl Paraoxon (Me-POX)

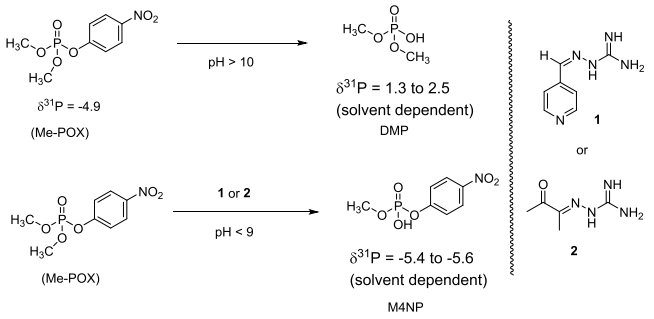

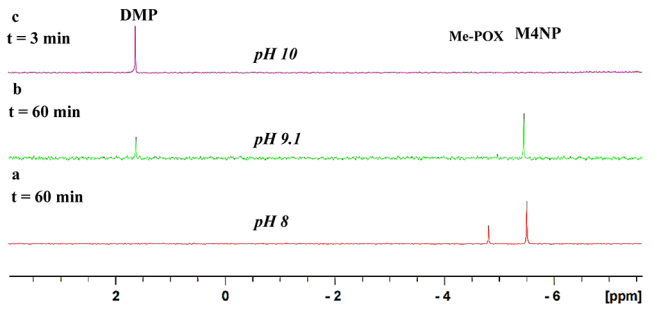

Figure 4. Proton-decoupled ^{31}P NMR (161.9 MHz) for the reaction of Me-POX with pyridine-4-aldehyde aminoguanidine imine (**1**); 2,3-butanedione aminoguanidine imine (**2**); and Dekon-139 (**3**) in 0.5 M borate buffer (in DMSO) at pH 8−10.

- at pH 8, M4NP is formed as the predominant product,
- at relatively high pH (pH 10), DMP is formed as the predominant product;
- at intermediate pH (pH 9.1), M4NP as well as DMP are observed as the hydrolytic products of Me-POX.

The formation of DMP as the exclusive product at relatively high pH implies an S_N2-like reaction with the 4-nitrophenyloxy group acting as the leaving group (Figure 6a). The predominant formation of M4NP in the hydrolysis of Me-POX at relatively low pH may be rationalized by reversible protonation of the relatively more basic methoxy oxygen by the generated aminoguanidinium moiety (Figure 6b), over that of the aryloxy oxygen. Thus, the protonated methoxy group acts as a relatively better leaving group compared to the 4-nitrophenoxyl group to give M4NP as the major product under relatively acidic conditions (Figures 5a and 6).

The hydrolytic breakdown of Me-POX becomes significantly slower as the basicity of the buffer medium is lowered. However, the aminoguanidine-derived aldimines **1** and **2**, as well as Dekon-139 (**3**), have a rate-enhancing effect on the hydrolysis of the Me-POX even under the relatively low basic conditions.

The reactivity of 4-pyridine carboxaldehyde aminoguanidine imine (1) and 2,3-butanedione aminoguanidine imine (2) toward protonation at moderately to high pH can be attributed to differences in the basicity of their imine nitrogen atoms. The imine nitrogen in **1** is more basic due to the electron-withdrawing effect of the pyridine ring, which enhances the electrophilicity of the nitrogen, making it more susceptible to protonation. This leads to a faster protonation reaction compared to that of **2**, where the methylene spacer between the imine group and the electron-withdrawing carbonyl group diminishes the electron-withdrawing effect, resulting in lower basicity of the imine nitrogen. Consequently, the imine nitrogen in the 2,3-butanedione aminoguanidine imine protonates more slowly, making this compound less reactive under similar alkaline conditions.

On the other hand, Dekon 139 (3) exhibits the least reactivity toward protonation in this series. The oxime group (−C═NOH) in Dekon 139 has a pK_a of approximately 9.3[46] at pH 10, meaning it remains largely in its deprotonated oximate form (C═NO$^-$) at higher pH. The oximate anion is a weak base and does not exhibit the same level of electrophilic reactivity as the amine or imine groups in the other two compounds. Its nucleophilicity tends to dominate its acid−base properties at these pH values. Thus, at pH 10, the oxime group is less prone to protonation, making Dekon 139 the least reactive of the three compounds at this pH. Even at neutral pH, its reactivity remains limited due to the lower protonation tendency of the oxime compared to that of the more basic amine or imine groups.

The kinetic studies of the hydrolytic breakdown of Me-POX by aminoguanidine-derived aldimines **1** and **2**, Dekon 139 (**3**), and alkaline water at various pH levels are depicted in Figure 5. Each plot illustrates the increase in Me-POX detoxification over time (min). Under identical reaction conditions, the kinetics of Me-POX degradation indicate that the aminoguanidine aldimines **1** and **2** are significantly more reactive than Dekon 139.

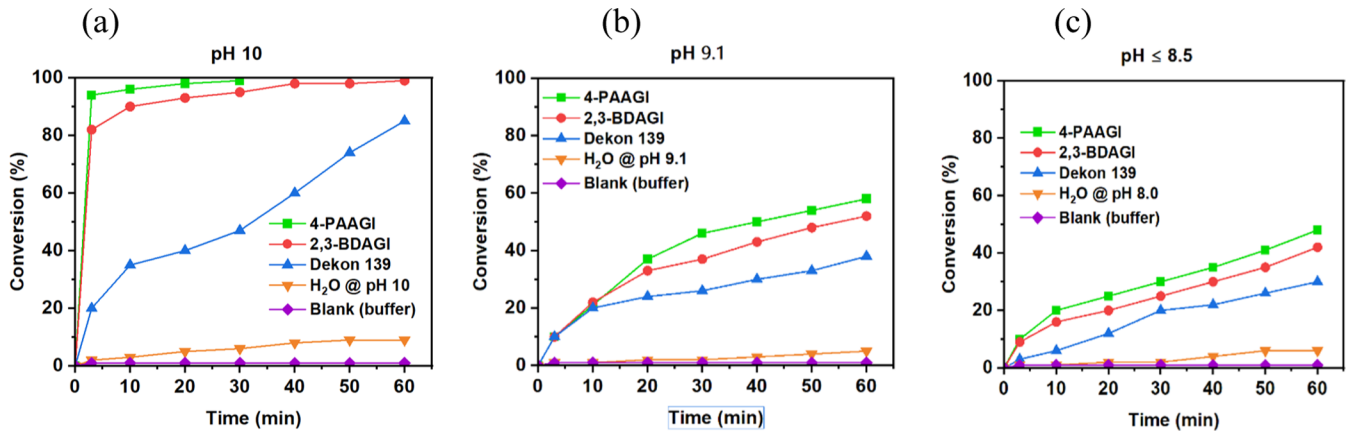

Figure 5. Time-course conversion of Me-POX (10 mM) to the nontoxic products in the presence of the aminoguanidine analogs -(**1**, 4-PAAGI, and **2**, 2,3-BDAGI), Dekon 139 (50 mM), and alkaline water in 1.0 M glycine-DMSO buffer at (a) pH 10, (b) pH 9, and (c) pH 8 at 25 °C.

https://doi.org/10.1021/acsomega.4c09946
ACS Omega 2025, 10, 12294−12305

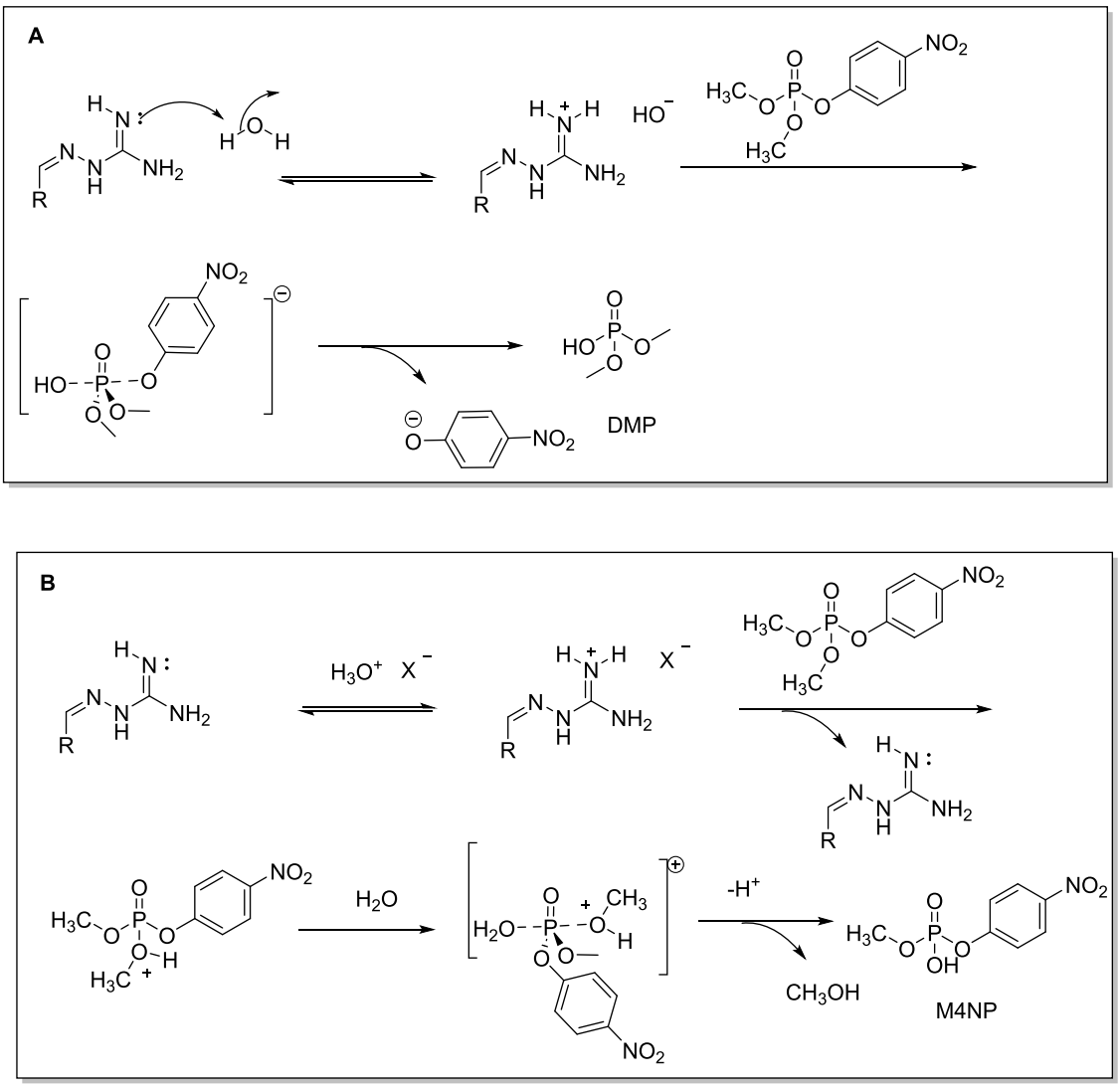

Figure 6. Proposed mechanism for the aminoguanidine aldimines-catalyzed hydrolysis of methyl paraoxon (Me-POX) at pH > 9 (A), and at pH < 9 (B).

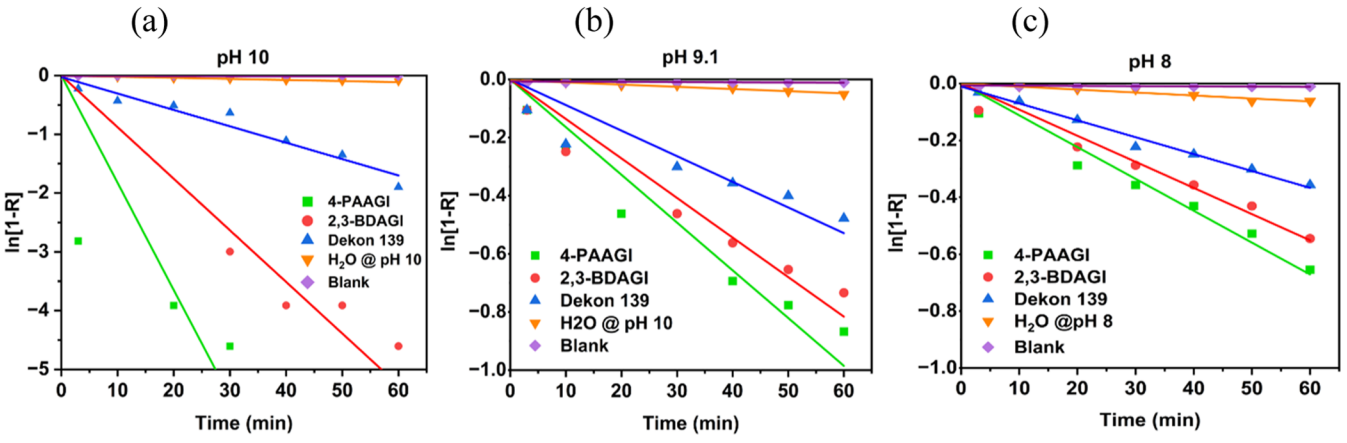

Figure 7. Prototypical first-order kinetic model for Me-POX (10 mM) conversion catalyzed by the aminoguanidine analogs (**1**, 4-PAAGI, and **2**, 2,3-BDAGI), Dekon 139 (50 mM), and alkaline Water in 1.0 M glycine-DMSO buffer at (a) pH 10, (b) pH 9, and (c) pH 8 at 25 °C.

For quantitative analysis, we evaluated the standard kinetic parameters for Me-POX hydrolysis at the various pH levels by applying different kinetic models to the collected data. Both first-order and second-order (Figure S23) kinetic models were employed to determine the best fit, evaluated by regression coefficients (R^2) and agreement with observed degradation. The calculated half-life values from either model indicate that first-order kinetics closely align with experimental outcomes.

https://doi.org/10.1021/acsomega.4c09946
ACS Omega 2025, 10, 12294−12305

Therefore, under pseudo-first-order conditions using eqs 2 and 3, with linear plots in $\ln[1 - R]$ versus time ($R^2 > 0.90$) (Figure 7), we quantified the decomposition half-life ($t_{1/2}$, min). As shown in Figure 7(a−c) and Table 1, aminoguanidine aldimines **1** and **2** exhibit higher k_{obsd} values and shorter half-lives, indicating greater reactivity. They demonstrated

- a 10-fold and 4-fold rate enhancement, respectively, compared to Dekon 139 and
- a 126-fold and 53-fold rate enhancement, respectively compared to the alkaline hydrolysis at a high pH 10.

In summary, these kinetic data support the proposed catalytic mechanism of Me-POX inactivation by the aminoguanidine moiety in **1** and **2** and highlight their enhanced reactivity for Me-POX degradation compared to Dekon-139, across all pH conditions studied.

It is instructive to note that the observed kinetics of Me-POX degradation at high pH 10, by **1** and **2** transitions from rapid initiation to a pseudo-first-order regime. This transition is characterized by an initial burst of reactivity of **1** and **2** leading to a significant conversion of Me-POX (94 and 83%, respectively), within a remarkably short period (<3 min) (Figure 5a). Upon analyzing the data obtained from the reaction kinetics, it becomes evident that the half-life of the reaction during the initial stages is exceptionally brief, emphasizing the highly catalytic activity of **1** and **2** on Me-POX compared to Dekon-139. The calculated half-life within the first few minutes of reaction, derived from the initial data points corresponding to approximately 94 and 83% conversion of Me-POX in the presence of **1** and **2**, was found to be 44 and 77 s, respectively. This contrasts starkly with the half-life calculated over a longer period using the first-order rate law, which led to 3.15 and 7.11 min, respectively.

We have further substantiated the structural assignments of the hydrolysis products based on the gauge-including atomic orbital (GIAO)-^{31}P NMR chemical shift calculations.[47] The GIAO-B3LYP-6-31G(d)//B3LYP-6-31G(d)-derived δ^{31}P for M4NP

- predicted (δ ^{31}P −5.5), DMP (δ^{31}P 3.6), and Me-POX (δ^{31}P −3.06) are in close agreement with
- the experimentally observed δ^{31}P −5.4 to −5.6, 1.3 to 2.5 (solvent dependent), and −4.9, respectively.

Our observed δ^{31}P for these compounds are also in accord with the reported chemical shifts.[48] At this level of theory, the GIAO δ^{31}P of Me-POX, −3.06 ppm, deviates from the observed chemical shift (δ^{31}P = −4.9) by about 1.5 ppm, whereas there is only a small discrepancy of δ^{31}P for DMP and M4NP between theory and experiment. We did not carry out the GIAO calculations using implicit solvation models because the gas phase NMR chemical shifts are already in good agreement with the experimental values.

We carried out density functional theory (DFT) calculations to rationalize the pH-dependent hydrolysis products of Me-POX in the gas phase. The proton affinities (PA) for the protonation of the aryloxy and methoxy oxygens were estimated as the negative enthalpies of the protonation reaction. Under standard temperature and pressure conditions (298 K and 1 atm pressure), the enthalpy of H^+ was estimated as 1.48 kcal mol^{-1} (i.e., 5/2 RT) and this enthalpy was used in the proton affinity calculations.[49] At the M06-2*X*/6-31+G(d,p) level of theory, the calculated proton affinities for the protonation of the methoxy oxygen and the aryloxy oxygen of Me-POX are 174.7 and 173.5 kcal mol^{-1}, respectively (Scheme 2).[50,51] Thus, protonation at the methoxy oxygen is favored over the aryloxy oxygen by 1.3 kcal mol^{-1}.

Based on these proton affinity calculations, it is evident that at relatively lower pH (pH < 9), the hydrolytic reaction of the Me-POX is initiated by the reversible protonation of the methoxy oxygen by the generated aminoguanidinium moiety in preference to that on the aryloxy oxygen, and thus at lower pH, the protonated methoxy group acts as a better leaving group, giving the observed M4NP as the major product (Figure 8).

At relatively high pH (pH 10), the hydrolytic reaction is dominated by the S_N2 reaction of the neutral substrate by the hydroxide anion (the counteranion of the aminoguanidinium moiety), affording the dimethyl phosphate (DMP) as the predominant product, through the departure of the relatively better leaving 4-nitrophenoxy group (4-NP), in preference to that of the methoxy moiety (Figure 5a). Thus, DFT calculations were performed by using the M06-2*X*/6-31G(d)//B3LYP/6-31G(d) level of theory to elucidate the mechanism behind the rapid decontamination observed in the aminoguanidine-assisted hydrolysis of Me-POX under alkaline conditions. The reaction's enthalpy (ΔH), entropy (ΔS), and Gibbs free energy (ΔG) profiles in solution were examined. The reaction pathway, which involves the nucleophilic attack of the aminoguanidinium counterion (OH^-) on Me-POX, is illustrated in Figure 9.

Table 1. Observed First-Order Rate Constant (k_{obs}) and Half-Life ($t_{1/2}$) for Me-POX Degradation Catalyzed by the Aminoguanidine Imine Analogs, Dekon 139, and Alkaline Water in 1.0 M Glycine-DMSO Buffer at Various pH at 25 °C

catalyst	rate constant k_{obs} (min^{-1})	$t_{1/2}$ (min)
	pH 10	
4-PAAGI (1)	0.2199	3.15
2,3-BDAGI (2)	0.0974	7.11
Dekon-139 (3)	0.0279	24.83
alkaline hydrolysis	0.0019	372.58
blank	7.7836×10^{-04}	890.35
	pH 9.1	
4-PAAGI (1)	0.01635	42.38
2,3-BDAGI (2)	0.01360	50.96
Dekon-139 (3)	0.00671	103.28
alkaline hydrolysis	0.00076	915.46
blank	7.783×10^{-04}	890.40
	pH < 8.5	
4-PAAGI (1)	0.01118	61.99
2,3-BDAGI (2)	0.00918	75.49
Dekon-139 (3)	0.00594	116.66
alkaline hydrolysis	0.00104	666.34
blank (buffer)	7.7836×10^{-04}	890.40

COMPUTATIONAL STUDY OF THE MECHANISM

The mechanism underlying the dramatically accelerated decontamination process was investigated using density functional theory (DFT) calculations (M06-2X-D3/6-31G+**) with the results shown in Figure 9. We find that **1** and **2** act as weak bases in solution, partially forming protonated ions, shown as **Int 1**. The catalysts facilitate nucleophilic attack by forming hydrogen bonds to build thermodynamically preferred transition state **TS 2** (at 10.7 kcal/mol for **1** and 12.3 kcal/mol for **2**). **TS 2** can be constructed either from the catalysts (**1** or **2**) and H_2O (**Sub**), or from the protonated catalysts (**1**-H^+ or **2**-H^+) and OH^- (**Int 1**). This demonstrates that in the presence of **1** or

https://doi.org/10.1021/acsomega.4c09946
ACS Omega 2025, 10, 12294−12305

Scheme 2. DFT-Calculated Proton Affinities (PA) for the Methyl Paraoxon (Me-POX)

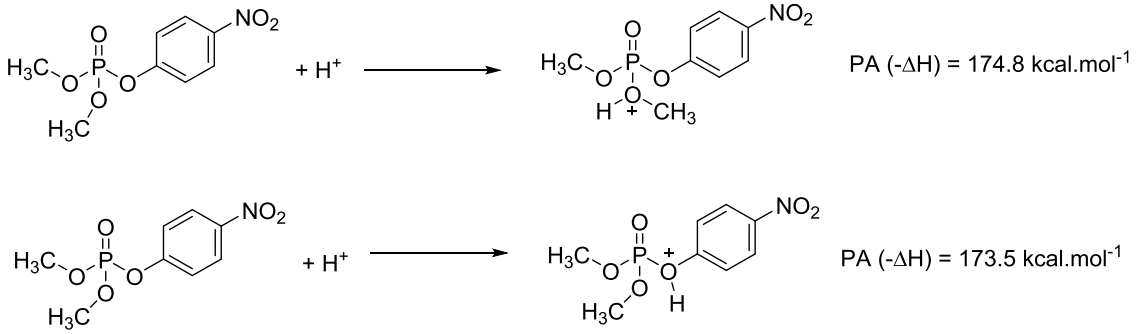

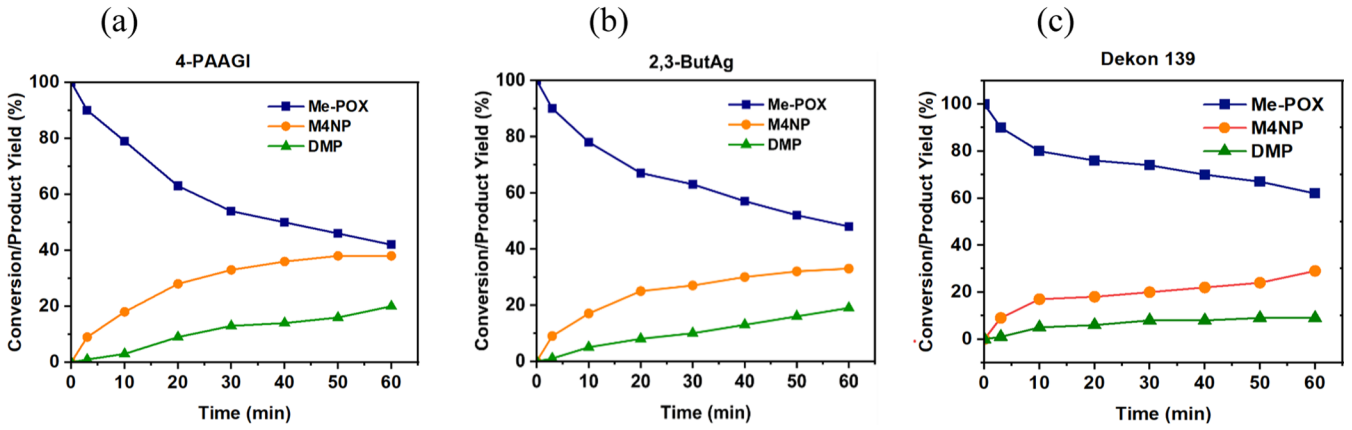

Figure 8. Product distribution of Me-POX (10 mM) degradation in 1.0 M glycine-DMSO buffer, (pH 9.1) catalyzed by the (a) 4-PAAGI (**1**) (50 mM), (b) 2,3-BDAGI (**2**) (50 mM), and (c) Dekon-139 (**3**) (50 mM) in 1.0 M glycine-DMSO buffer at 25 °C.

2, both hydroxide and water can actively participate in the substitution process.

Comparing to the uncatalyzed scenario, the catalysts both significantly lower the energy barrier of the original RDS **TS 1** while also expanding the active species to include H_2O. Without the assistance of **1** or **2**, H_2O alone lacks sufficient nucleophilicity to attack the Me-POX substrate. Thus, the catalysts enhance the decontamination efficiency by facilitating the involvement of water and reducing the activation energy of RDS by stabilizing the transition state. The decontamination mechanism of Dekon-139 (**3**) was investigated previously,[55] but we also calculated the energy. The RDS for **3** is **TS 3**, in which the anion of Dekon-139 attacks the phosphate center of the Me-POX substrate. The activation energy of this transition step is 16.1 kcal/mol, which is much lower than that of the uncatalyzed scenario but not nearly as low as that of the catalyzed **TS 2**. According to the Eyring equation, the rate constants of the RDS in the mechanism for **1** and **2** are estimated to be over 9100 times and 610 times faster, respectively, than the RDS for Dekon-139 decontamination.

CONCLUSIONS

In summary, we have designed relatively nontoxic and effective decontaminating agents for organophosphate nerve agents and pesticides that are substantially more reactive than the state-of-the-art decontaminating agent Dekon-139, the active ingredient of the Reactive Skin Decontaminating Lotion (RSDL). The aminoguanidine-derived aldimines **1** and **2** hydrolyzed Me-POX instantaneously at pH 10, whereas under otherwise similar conditions, Dekon-139 was a substantially less effective catalyst. The observed pH-dependent product distribution of the Me-POX hydrolysis, in the presence of catalysts **1** and **2**, was rationalized through DFT calculations. Thus, the computed proton affinity for the methoxy oxygen is relatively higher than that of the aryloxy oxygen by about 1.3 kcal/mol, and the protonated methoxy moiety thereby serves as a relatively better leaving group, resulting in M4NP as the major product (relatively nontoxic) under relatively acidic conditions at pH 8.5. However, under relatively more basic conditions (pH 10), Me-POX gives predominantly DMP as the hydrolytic product (relatively nontoxic) through a concerted S_N2 reaction. The DFT-calculated mechanisms indicate that **1** and **2** form hydrogen bonds to lower the activation energy of the RDS, therefore accelerating the hydrolysis process.

Importantly, while specific toxicity data for these compounds (**1** and **2**) are not yet available from our laboratory, existing literature supports the inference of their nontoxicity,[43,52] paving the way for future studies aimed at confirming this assertion. These studies collectively demonstrate that aminoguanidine-derived aldimines **1** and **2** provide safer and substantially more effective decontaminating agents for nerve agents and pesticides compared to the state-of-the-art surface decontaminating agent, Dekon-139 (**3**).

MATERIALS AND ANALYTICAL METHODS

Materials. Deuterated solvent, dimethyl sulfoxide-d_6 (DMSO-d_6, ≥99.5%), 4-pyridine carboxaldehyde (C_6H_5NO, ≥99.0%), and 2,3−butanedione ($C_6H_4O_2$, ≥99.5%) were purchased from A2B Chemicals (America) and used without further purification. The following chemicals were also purchased from commercial vendors: Methyl paraoxon (DMNP - $C_8H_{10}NO_6P$, ≥99.0%, TCL, America), Amino-

https://doi.org/10.1021/acsomega.4c09946
ACS Omega 2025, 10, 12294−12305

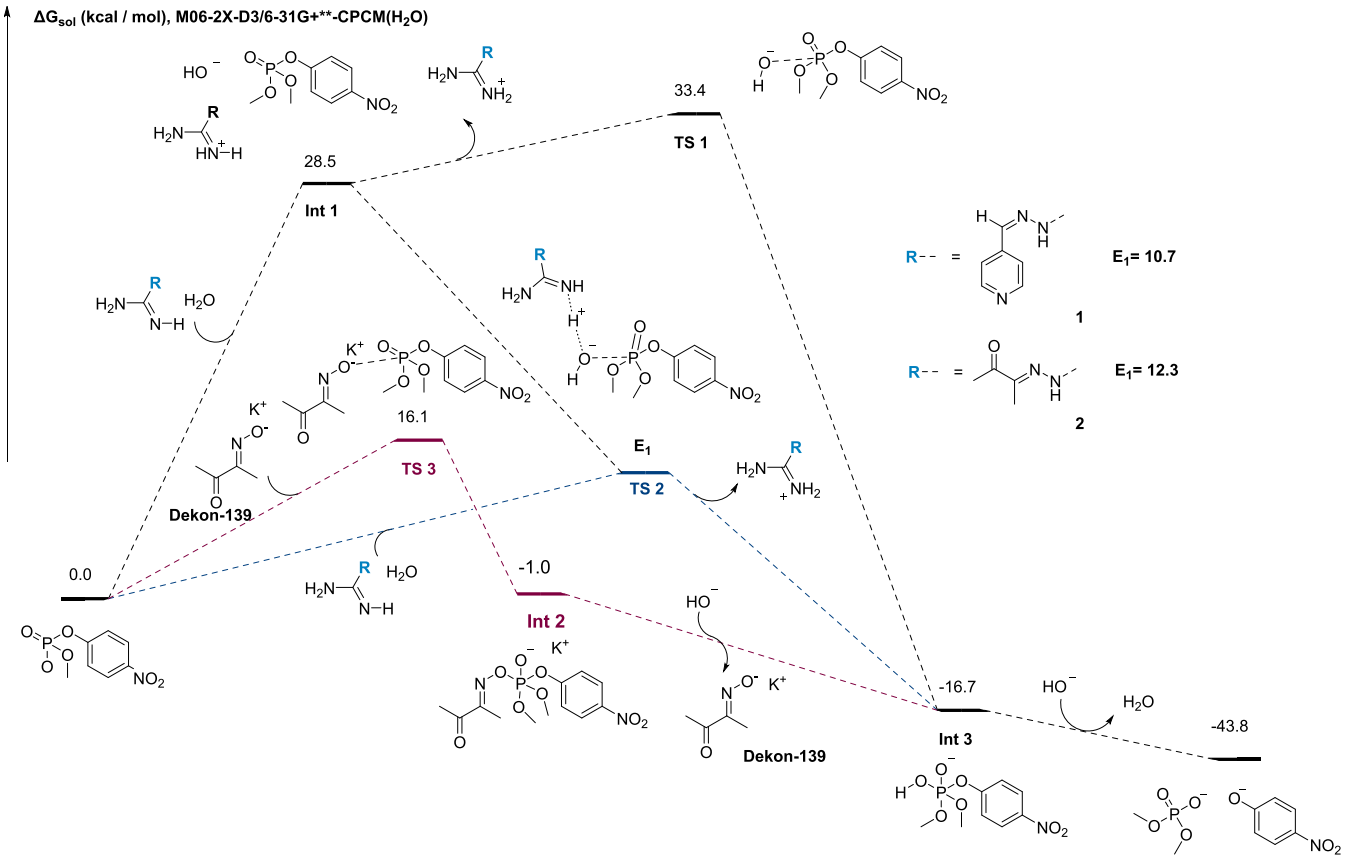

Figure 9. DFT (M06-2X-D3/6-31G+**) computed free energy profile of the Me-POX hydrolysis mechanism with (blue) and without **1** and **2** and **Dekon-139** decontamination (red).

guanidine bicarbonate ($C_2H_8N_4O_3$, ≥99.0%, AK Scientific), methanol (CH_4O, ≥98.0, Fisher Scientific), ethanol (C_2H_6O, ≥98.0%, Fisher Scientific), Glycine ($C_2H_5NO_2$, ≥99.0%, Fisher Scientific), dimethyl sulfoxide (DMSO, ≥99.0%, Sigma-Aldrich), sodium hydroxide (Sigma-Aldrich), sulfuric acid solution (H_2SO_4, ≥99.5%, Fisher Scientific), chloroform-*d* ($CDCl_3$, ≥99.0%, Fisher Scientific), magnesium sulfate anhydrous ($MgSO_4$, ≥99.9%, Macklin), 2-amino-2-methyl-1,3-propanediol ($C_4H_{11}NO_2$, ≥98.0%, Fisher Scientific), and boric acid (BH_3O_3, ≥99.5%, Fisher Scientific).

Analytical Methods. The structural identity of compounds was confirmed by NMR spectroscopy. Chemical shift (δ) values for NMR spectra are reported in parts per million relative to tetramethylsilane (TMS), set as an internal standard (δ = 0.00 ppm).

Synthesis Methods. *Synthesis of Compounds (**1, 2, and 3**).* The aminoguanidine-derived aldimines 1 and 2, and Dekon-139 (3) were synthesized according to published methods with slight modifications.[43]

Pyridine-4-carboxaldehyde Aminoguanidine Imine (1, 4-PAAG1). To a mixture of 4-pyridine carboxaldehyde (0.5 g, 4.1 mmol) and aminoguanidine bicarbonate (0.84 g, 6.18 mmol, 1.5 equiv) in 10 mL of ethanol was added 10% hydrochloric acid (1.0 mL) at room temperature. The mixture was refluxed at 70 °C with continuous stirring for 6 h. The obtained solution was cooled and neutralized with sodium bicarbonate. Ethanol was removed in vacuo, and the residue was washed with water, filtered, and then recrystallized from ethanol to give 4-pyridine carboxaldehyde aminoguanidine imine as a pale-yellow solid (1.38 g, 8.46 mmol, 85%). NMR spectra are given in Supporting Information.

^{1}H NMR; (400 MHz, DMSO- d_6) δ 8.43−8.41 (2Hm, ArH), 7.88 (1H, s, CHN), 7.57−7.55 (2H, d, ArH, 2H), 6.11−5.77 (NH)

^{13}C NMR. ^{13}C NMR. (100 MHz, DMSO- d_6) δ (161.74, 149.61, 144.25, 139.90, 120.26).

2,3-Butanedione Aminoguanidine Imine (2, 2,3-BDAGI). To a mixture of 2,3-butanedione (0.86 g, 10 mmol) and aminoguanidine bicarbonate (1.36 g, 10 mmol, 1 equiv) in 25 mL of a water−ethanol solvent (1:5) was added acetic acid (0.6 mL, 10 mmol, 1 equiv) at room temperature. The mixture was refluxed at 70 °C with continuous stirring for 4 h. The obtained solution was cooled and neutralized with sodium bicarbonate. Ethanol was removed in vacuo; water was then added to the residue and extracted with dichloromethane (3 × 10 mL). The combined organic layer was dried over anhydrous sodium sulfate and filtered, and the solvent was removed in vacuo to give 2,3-butanedione aminoguanidine imine as a yellow solid (1.28 g, 9.0 mmol, 90%). NMR spectra are given in Supporting Information.

^{1}H NMR; (400 MHz, DMSO- d_6) δ 11.42 (1H, s, NH), 8.08 (1H, s NH), 6.93 (2H, NH_2), 2.7 (3H), 2.2 (3H)

^{13}C NMR; (100 MHz, DMSO- d_6) δ (162.20, 159.04, 147.19, 21.23, 18.12).

2,3-Butanedione Monoxime (3, Dekon-139). To a mixture of 2,3-butanedione (0.86 g, 10 mmol) and hydroxylamine hydrochloride (0.695 g, 10 mmol, 1 equiv) in 20 mL of ethanol at 0 °C was added pyridine (0.89 g, 11 mmol) dropwise with stirring over 2 min. The mixture was refluxed at 70 °C with continuous stirring for 6 h, cooled to room temperature, and

https://doi.org/10.1021/acsomega.4c09946
ACS Omega 2025, 10, 12294−12305

filtered to remove the pyridine hydrochloride, and the solvent was removed in vacuo. Water was then added to the residue and extracted with ethyl acetate (3 × 10 mL) and the combined organic layer was dried over anhydrous sodium sulfate, filtered, and the solvent removed in vacuo. Dekon-139 obtained as a white solid (0.92 g, 9.10 mmol, 92%). NMR spectra are given in Supporting Information.

^{1}H NMR; (400 MHz, DMSO- d_6): δ 12.48 (1H, s, NOH), δ 2.2 (3H), 2.01 (3H)

^{13}C NMR; (100 MHz, DMSO- d_6): δ (196.70, 155.19, 24.89, 7.93).

NMR Spectroscopy. *Characterizations.* ^{1}H-, ^{13}C-, and ^{31}P NMR spectra were recorded on a Bruker Avance III-400 spectrometer (400 MHz for ^{1}H, 100 MHz for ^{13}C, and 162 MHz for ^{31}P) in $CDCl_3$ or DMSO-d_6 for the synthesized aminoguanidine analogs and Dekon-139. ^{1}H NMR, and ^{13}C NMR chemical shifts are referenced to the residual solvent signals in the deuterated solvents, and the ^{31}P chemical shifts are referenced to H_3PO_4; $\delta^{31}P = 0$.

Preparation of Buffer Solutions. The respective pH of buffer solutions was prepared in deuterated organic solvents and water (DI water), and their corresponding pH were measured using an Orion Star A211 pH Meter from Thermo scientific.

Preparation of 1.0 M Glycine-DMSO Buffer (pH 9.8). 1.5 g of glycine and 0.36 g of NaOH were dissolved in 20 mL of mixture of water and deuterated DMSO (1:4 ratio) to get 1.0 M Glycine-DMSO buffer. The pH of the buffer was adjusted to 9.8 using a dilute NaOH solution. The buffer was tightly sealed and stored for use.

The experimental hydrolysis of methyl paraoxon by the aminoguanidine imine analogs was carried out in glycine-DMSO, and borate-DMSO buffer solutions.

Catalytic Hydrolysis of Me-POX by Imines. A known amount of the catalysts (aminoguanidine-derived aldimines and Dekon-139) was weighed and dissolved in the buffer solution at the respective pH to obtain 50 mM solution (5 equiv toward Me-POX). Methyl paraoxon (Me-POX, 3.6 μL) was also dissolved in 2 mL of the buffer at the respective pH to achieve 10 mM solution. The hydrolysis profiles of methyl paraoxon were assessed in situ by liquid-state ^{31}P NMR spectroscopy using a Bruker Avance III 400 spectrometer (161.9 MHz) and the spectra analyzed using Topsin 4.3 software. All of the reactions were performed at ambient temperature. Deuterated DMSO (for lock and shimming) was used as NMR solvent for all experiments.

To a 5 mm diameter 8 in. long NMR tube, 0.5 mL of 50 mM catalysts (aminoguanidine analog) was transferred. 0.5 mL of 10 mM of the nerve agent simulant, methyl paraoxon, was then added and shaken for 10 s. The mixture was quickly kept under ^{31}P NMR (proton decoupled) analysis at different time intervals. The spectra were recorded at 25 °C by 32 scans with delay time of 2 s until methyl paraoxon was completely hydrolyzed. The relative rates of hydrolysis of Me-POX to dimethyl phosphate (DMP) by the catalysts were determined by ^{31}P[^{1}H] NMR spectroscopy from the relative integrations of their characteristic peaks.

Me-POX Degradation Kinetics. The degradation kinetics of Me-POX hydrolysis catalyzed by the aminoguanidine-derived aldimines and Dekon 139 as well as the alkaline water (Milli-Q) were evaluated using liquid-state ^{31}P NMR spectroscopy on a Bruker Avance III HD 400 spectrometer operating at 161.98 MHz The extent of reaction conversion (denoted as R) at various time points was determined by analyzing the ratio of the integrated signal of the hydrolysis product (dimethyl phosphate, DMP and/or methyl-4-nitrophenyl phosphate, M4NP) to the sum of the integrated ^{31}P signals of both the product(s) and the reactant (Me-POX) in ^{31}P NMR, expressed by eq 1

$$R = \Sigma I_p/(\Sigma I_r + \Sigma I_p) \quad (1)$$

where $\sum I_r$ and $\sum I_p$ are the sums of signal integrations corresponding to Me-POX (reactant) and DMP/M4NP (products), respectively. The kinetics of the reaction were found to follow pseudo-first-order kinetics, as described by eq 2. The observed rate constant (k_{obs}) was determined from the initial slope of linear plots of $\ln[1 - R]$ versus time (t). Each value of k_{obs} is the mean of three independent determinations with a RSD of no more than 2.5% RSD.

$$\ln[1 - R] = -k_{obs} \cdot t \quad (2)$$

wherein the reaction half-life ($t_{1/2}$) was derived using eqs 3.

$$t_{1/2} = \ln(2)/k_{obs} \quad (3)$$

DFT Calculations. DFT calculations of the proton affinities for the Me-POX and the GIAO NMR chemical shift calculations of the Me-POX and its hydrolyzed products were performed in the gas phase, as implemented in the Gaussian-16 program.[53] The proton affinities were computed at the M06-2X/6-31G +(d,p) level of theory with Grimme D3 London Dispersion corrections.[54] The enthalpy of formation of H^+ is taken as 5/2 RT, which under standard temperature and pressure conditions is 1.48 kcal mol^{-1}.[49] The GIAO NMR chemical shift calculations were performed at the GIAO-B3LYP/6-31g(d)//B3LYP/6-31g(d) level of theory in the gas phase.[47] The validity of the true minima of the optimized structures was verified through frequency calculations at the same level of theory (all positive vibrational frequencies). The total free energies (G_{Tot}) and enthalpies (H_{Tot}) of the molecules were derived from the vibrational frequency calculations (unscaled) at the same level of calculations, at 298.15 K.

The mechanism calculations were performed using the Jaguar software version 10.9 from Schrodinger Inc.[56] The structure optimizations were performed using the hybrid M06-2X/6-31G +** level of DFT including the Grimme D3 London Dispersion corrections and the CPCM implicit solvation model[57] implemented in Jaguar. Vibrational frequency calculations at 298.15 K were performed at the same level. In these gas phase calculations, there are 3 translational degrees of freedom (dof) and 3 rotational dof leading to large entropies, but in solvent these dof become hindered librational dof, reducing the entropy by 40 to 60%. This becomes an issue for reactions that change the number of molecules. To account for this entropy loss, a correction is often applied to translational and rotational modes.[58] We assume in this paper a factor of 50%. This entropy correction is implemented via the following formula

$$G = H - T \times (0.5 \times (S_{tran} + S_{rot}) + S_{vib} + S_{elec}) \quad (4)$$

The proton affinities were computed at the M06-2X/6-31G +(d,p) level of theory with the Grimme D3 London Dispersion corrections. The enthalpy of formation of H^+ is taken as 5/2 RT, which under standard temperature and pressure conditions is 1.48 kcal mol^{-1}.[48] The GIAO NMR chemical shift calculations were performed at the GIAO-B3LYP/6-31g(d)//B3LYP/6-31g(d) level of theory in the gas phase.[46] The validity of the true minima of the optimized structures was verified through frequency calculations at the same level of theory (all positive

https://doi.org/10.1021/acsomega.4c09946
ACS Omega 2025, 10, 12294−12305

vibrational frequencies). The total free energies (G_{Tot}) and enthalpies (H_{Tot}) of the molecules were derived from the vibrational frequency calculations (unscaled) at the same level of calculations, at 298.15 K.

■ ASSOCIATED CONTENT

Supporting Information

The Supporting Information is available free of charge at https://pubs.acs.org/doi/10.1021/acsomega.4c09946.

Synthesis procedures of aminoguanidine-derived aldimines used in this study, ^{1}H and ^{13}C NMR spectra of decontaminants, GC-MS chromatograms, schematic illustration of the Methyl Paraoxon (Me-POX) decontamination evaluation procedure, ratios (as percentages) of chemically decontaminated Me-POX after reaction of aminoguanidine imines at different pH conditions, Me-Pox hydrolysis kinetics of aminoguanidine imines under different pH conditions over time, linear plots between $\ln(1 - R)$ versus time, mechanism of Me-POX hydrolysis by aminoguanidine imines, DFT and GIAO calculations of Me-POX hydrolysis, figures and tables, coordinates for structures in mechanisms (PDF)

■ AUTHOR INFORMATION

Corresponding Authors

William A. Goddard, III − *Materials and Process Simulation Center (MSC), California Institute of Technology, Pasadena, California 91125, United States;* orcid.org/0000-0003-0097-5716; Email: wag@caltech.edu

V. Prakash Reddy − *Department of Chemistry, Missouri University of Science and Technology, Rolla, Missouri 65409, United States; Materials and Process Simulation Center (MSC), California Institute of Technology, Pasadena, California 91125, United States;* orcid.org/0000-0003-3011-4175; Phone: (573)341-4768; Email: preddy@mst.edu

Authors

Emmanuel Kingsley Darkwah − *Department of Chemistry, Missouri University of Science and Technology, Rolla, Missouri 65409, United States*

Puspa Aryal − *Department of Chemistry, Missouri University of Science and Technology, Rolla, Missouri 65409, United States*

Chi Zhang − *Materials and Process Simulation Center (MSC), California Institute of Technology, Pasadena, California 91125, United States*

Charles B. Musgrave, III − *Materials and Process Simulation Center (MSC), California Institute of Technology, Pasadena, California 91125, United States;* orcid.org/0000-0002-3432-0817

Complete contact information is available at: https://pubs.acs.org/10.1021/acsomega.4c09946

Notes

The authors declare no competing financial interest.

■ ACKNOWLEDGMENTS

V.P.R. gratefully acknowledges the funding from the Department of Defense (W911NF-21-2-0259). W.A.G. acknowledges funding from ONR (N00014-23-1-2105).

■ DEDICATION

[§]Passed away April 18, 2024

■ REFERENCES

(1) Brooks, J.; Erickson, T. B.; Kayden, S.; Ruiz, R.; Wilkinson, S.; Burkle, F. M., Jr. Responding to chemical weapons violations in Syria: legal, health, and humanitarian recommendations. *Conflict Health* **2018**, *12*, No. 12.

(2) Aas, P. Future considerations for the medical management of nerve-agent intoxication. *Prehospital Disaster Med.* **2003**, *18*, 208−216.

(3) McGuire, J. R.; Bester, S. M.; Guelta, M. A.; Cheung, J.; Langley, C.; Winemiller, M. D.; Bae, S. Y.; Funk, V.; Myslinski, J. M.; Pegan, S. D.; Height, J. J. Structural and Biochemical Insights into the Inhibition of Human Acetylcholinesterase by G-Series Nerve Agents and Subsequent Reactivation by HI-6. *Chem. Res. Toxicol.* **2021**, *34*, 804−816.

(4) Lenz, D. E.; Cerasoli, D.; Maxwell, D. M. Radiolabelled soman binding to sera from Rats, Guinea Pigs and Monkeys. *Toxicol. Lett.* **2018**, *283*, 86−90.

(5) Mercey, G.; Verdelet, T.; Renou, J.; Kliachyna, M.; Baati, R.; Nachon, F.; Jean, L.; Renard, P.-Y. Reactivators of acetylcholinesterase inhibited by organophosphorus nerve agents. *Acc. Chem. Res.* **2012**, *45*, 756−766.

(6) Eubanks, L. M.; Dickerson, T. J.; Janda, K. D. Technological advancements for the detection of and protection against biological and chemical warfare agents. *Chem. Soc. Rev.* **2007**, *36*, 458−470.

(7) Yang, Y. C.; Baker, J. A.; Ward, J. R. Decontamination of chemical warfare agents. *Chem. Rev.* **1992**, *92*, 1729−1743.

(8) Bromberg, L.; Hatton, T. A. Nerve Agent Destruction by Recyclable Catalytic Magnetic Nanoparticles. *Ind. Eng. Chem. Res.* **2005**, *44*, 7991−7998.

(9) Wagner, G. W.; Peterson, G. W.; Mahle, J. J. Effect of Adsorbed Water and Surface Hydroxyls on the Hydrolysis of VX, GD, and HD on Titania Materials: The Development of Self-Decontaminating Paints. *Ind. Eng. Chem. Res.* **2012**, *51*, 3598−3603.

(10) Bai, Y.; Dou, Y.; Xie, L.-H.; Rutledge, W.; Li, J.-R.; Zhou, H.-C. Zr-based metal-organic frameworks: design, synthesis, structure, and applications. *Chem. Soc. Rev.* **2016**, *45*, 2327−2367, DOI: 10.1039/c5cs00837a.

(11) Furukawa, H.; Cordova, K. E.; O'Keeffe, Michael.; Yaghi, O. M. The Chemistry and Applications of Metal-Organic Frameworks. *Science* **2013**, *341*, No. 1230444.

(12) Li, P.; Moon, S.-Y.; Guelta, M. A.; Harvey, S. P.; Hupp, J. T.; Farha, O. K. Encapsulation of a Nerve Agent Detoxifying Enzyme by a Mesoporous Zirconium Metal−Organic Framework Engenders Thermal and Long-Term Stability. *J. Am. Chem. Soc.* **2016**, *138*, 8052−8055.

(13) Bromberg, L.; Schreuder-Gibson, H.; Creasy, W. R.; McGarvey, D. J.; Fry, R. A.; Hatton, T. A. Degradation of Chemical Warfare Agents by Reactive Polymers. *Ind. Eng. Chem. Res.* **2009**, *48*, 1650−1659.

(14) Bromberg, L.; Pomerantz, N.; Schreuder-Gibson, H.; Hatton, T. A. Degradation of Chemical Threats by Brominated Polymer Networks. *Ind. Eng. Chem. Res.* **2014**, *53*, 18761−18774.

(15) Hartmann-Thompson, C.; Hu, J.; Kaganove, S. N.; Keinath, S. E.; Keeley, D. L.; Dvornic, P. R. Hydrogen-Bond Acidic Hyperbranched Polymers for Surface Acoustic Wave (SAW) Sensors. *Chem. Mater.* **2004**, *16*, 5357−5364.

(16) Wang, S.; Pomerantz, N. L.; Dai, Z.; Xie, W.; Anderson, E. E.; Miller, T.; Khan, S. A.; Parsons, G. N. Polymer of intrinsic microporosity (PIM) based fibrous mat: combining particle filtration and rapid catalytic hydrolysis of chemical warfare agent simulants into a highly sorptive, breathable, and mechanically robust fiber matrix. *Mater. Today Adv.* **2020**, *8*, No. 100085.

(17) Biswas, P.; Shuster, D. B.; Baghirzade, B. S.; Scanga, R. A.; Harris, S. A.; Tran, C. N.; Apul, O. G.; Reuther, J. F. Oxime-Functionalized, Nonwoven Nanofabrics for Rapid, Inexpensive Decontamination of Nerve Agent Simulant. *ACS Appl. Nano Mater.* **2023**, *6*, 3425−3434.

(18) Wilson, C.; Cooper, N. J.; Briggs, M. E.; Cooper, A. I.; Adams, D. J. Investigating the breakdown of the nerve agent simulant methyl

paraoxon and chemical warfare agents GB and VX using nitrogen containing bases. *Org. Biomol. Chem.* **2018**, *16*, 9285−9291.
(19) Moon, S. Y.; Liu, Y.; Hupp, J. T.; Farha, O. K. Instantaneous hydrolysis of nerve-agent simulants with a six-connected zirconium-based metal-organic framework. *Angew. Chem., Int. Ed.* **2015**, *54*, 6795−6799.
(20) Mondloch, J. E.; Katz, M. J.; Isley, W. C., III; Ghosh, P.; Liao, P.; Bury, W.; Wagner, G. W.; Hall, M. G.; DeCoste, J. B.; Peterson, G. W.; Snurr, R. Q.; Cramer, C. J.; Hupp, J. T.; Farha, O. K. Destruction of chemical warfare agents using metal−organic frameworks. *Nat. Mater.* **2015**, *14*, 512−516.
(21) Moon, S.-Y.; Proussaloglou, E.; Peterson, G. W.; DeCoste, J. B.; Hall, M. G.; Howarth, A. J.; Hupp, J. T.; Farha, O. K. Detoxification of Chemical Warfare Agents Using a Zr6-Based Metal−Organic Framework/Polymer Mixture. *Chem. - Eur. J.* **2016**, *22*, 14864−14868.
(22) Užarević, K.; Wang, T. C.; Moon, S.-Y.; Fidelli, A. M.; Hupp, J. T.; Farha, O. K.; Friščić, T. Mechanochemical and solvent-free assembly of zirconium-based metal−organic frameworks. *Chem. Commun.* **2016**, *52*, 2133−2136.
(23) Turetsky, D.; Alzate-Sánchez, D. M.; Wasson, M. C.; Yang, A.; Noh, H.; Atilgan, A.; Islamoglu, T.; Farha, O. K.; Dichtel, W. R. Hot Press Synthesis of MOF/Textile Composites for Nerve Agent Detoxification. *ACS Mater. Lett.* **2022**, *4*, 1511−1515.
(24) Kalaj, M.; Palomba, J. M.; Bentz, K. C.; Cohen, S. M. Multiple functional groups in UiO-66 improve chemical warfare agent simulant degradation. *Chem. Commun.* **2019**, *55*, 5367−5370.
(25) de Koning, M. C.; van Grol, M.; Breijaert, T. Degradation of Paraoxon and the Chemical Warfare Agents VX, Tabun, and Soman by the Metal-Organic Frameworks UiO-66-NH2, MOF-808, NU-1000, and PCN-777. *Inorg. Chem.* **2017**, *56*, 11804−11809.
(26) Zammataro, A.; Santonocito, R.; Pappalardo, A.; et al. Catalytic Degradation of Nerve Agents. *Catalysts* **2020**, *10*, No. 881, DOI: 10.3390/catal10080881.
(27) Rezaee, T.; Fazel-Zarandi, R.; Karimi, A.; Ensafi, A. A. Metal-organic frameworks for pharmaceutical and biomedical applications. *J. Pharm. Biomed. Anal.* **2022**, *221*, No. 115026.
(28) Fentabil, M.; Gebremedhin, M.; Barry, J.; Mikler, J.; Cochrane, L. In vivo efficacy of the Reactive Skin Decontamination Lotion (RSDL) kit against organophosphate and carbamate pesticides. *Chem.-Biol. Interact.* **2020**, *318*, No. 108980.
(29) Magnano, G. C.; Rui, F.; Filon, F. L. Skin decontamination procedures against potential hazards substances exposure. *Chem.-Biol. Interact.* **2021**, *344*, No. 109481.
(30) Feschuk, A. M.; Law, R. M.; Maibach, H. I. Comparative efficacy of Reactive Skin Decontamination Lotion (RSDL): A systematic review. *Toxicol. Lett.* **2021**, *349*, 109−114.
(31) Fryer, M. W.; Gage, P. W.; Neering, I. R.; Dulhunty, A. F.; Lamb, G. D. Paralysis of skeletal muscle by butanedione monoxime, a chemical phosphatase. *Pfluegers Arch. Eur. J. Physiol.* **1988**, *411*, 76−79.
(32) Yagi, N.; Takemori, S.; Watanabe, M.; Horiuti, K.; Amemiya, Y. Effects of 2,3-butanedione monoxime on contraction of frog skeletal muscles: an x-ray diffraction study. *J. Muscle Res. Cell Motil.* **1992**, *13*, 153−160.
(33) Walters, T. J.; Kauvar, D. S.; Reeder, J.; Baer, D. G. Effect of reactive skin decontamination lotion on skin wound healing in laboratory rats. *Mil. Med.* **2007**, *172*, 318−321.
(34) Reactive Skin Decontamination Lotion (RSDL) - Medical Countermeasures Database. https://chemm.hhs.gov/countermeasure_RSDL.htm
(35) Prasad, K.; Mishra, M. Do Advanced Glycation End Products and Its Receptor Play a Role in Pathophysiology of Hypertension? *Int. J. Angiol.* **2017**, *26*, 1−11.
(36) Borg, D. J.; Forbes, J. M. Targeting advanced glycation with pharmaceutical agents: where are we now? *Glycoconjugate J.* **2016**, *33*, 653−670.
(37) Spadaccio, C.; Nenna, A.; Nappi, F.; Singh, S. S. A.; Sutherland, F. W.; Di Domenico, F.; Chello, M. Pharmacologic Approaches Against Advanced Glycation End Products (AGEs) in Diabetic Cardiovascular Disease. *Res. Cardiovasc. Med.* **2015**, *4*, No. e26949.
(38) Turgut, F.; Bolton, W. K. Potential new therapeutic agents for diabetic kidney disease. *Am. J. Kidney Dis.* **2010**, *55*, 928−940.
(39) Vasan, S.; Foiles, P.; Founds, H. Therapeutic potential of breakers of advanced glycation end product-protein crosslinks. *Arch. Biochem. Biophys.* **2003**, *419*, 89−96.
(40) Menè, P.; Festuccia, F.; Pugliese, F. Clinical potential of advanced glycation end-product inhibitors in diabetes mellitus. *Am. J. Cardiovasc. Drugs* **2003**, *3*, 315−320.
(41) Kim, E. C. H.-O.; Jung, S.-H.; Kim, J. H.; Lee, J.-M.; Suh, B.-C.; Xiang, M. X.; Rhee, C. K. Improvement of therapeutic index of phosphodiesterase type IV inhibitors as anti-asmathics. *Bioorg. Med. Chem. Lett.* **2003**, *13*, 2355−2358.
(42) Leite, A. C. L.; de M Moreira, D. R.; Coelho, L. C. D.; de Menezes, F. D.; Brondani, D. J. Synthesis of aryl-hydrazones via ultrasound irradiation in aqueous medium. *Tetrahedron Lett.* **2008**, *49*, 1538−1541.
(43) Vaillancourt, V. A.; Larsen, S. D.; Tanis, S. P.; Burr, J. E.; Connell, M. A.; Cudahy, M. M.; Evans, B. R.; Fisher, P. V.; May, P. D.; Meglasson, M. D.; Robinson, D. D.; Stevens, F. C.; Tucker, J. A.; Vidmar, T. J.; Yu, J. H. Synthesis and Biological Activity of Aminoguanidine and Diaminoguanidine Analogues of the Antidiabetic/Antiobesity Agent 3-Guanidinopropionic Acid. *J. Med. Chem.* **2001**, *44*, 1231−1248.
(44) Gutiérrez, R. U.; Rebollar, A.; Bautista, R.; Pelayo, V.; Vargas, J. L.; Montenegro, M. M.; Espinoza-Hicks, C.; Ayala, F.; Bernal, P. M.; Carrasco, C.; Zepeda, L. G.; Delgado, F.; Tamariz, J. Functionalized α-oximinoketones as building blocks for the construction of imidazoline-based potential chiral auxiliaries. *Tetrahedron: Asymmetry* **2015**, *26*, 230−246.
(45) Piemontese, L.; Cerchia, C.; Laghezza, A.; Ziccardi, P.; Sblano, S.; Tortorella, P.; Iacobazzi, V.; Infantino, V.; Convertini, P.; Dal Piaz, F.; Lupo, A.; Colantuoni, V.; Lavecchia, A.; Loiodice, F. New diphenylmethane derivatives as peroxisome proliferator-activated receptor alpha/gamma dual agonists endowed with anti-proliferative effects and mitochondrial activity. *Eur. J. Med. Chem.* **2017**, *127*, 379−397.
(46) Wong, P. T.; Bhattacharjee, S.; Cannon, J.; Tang, S.; Yang, K.; Bowden, S.; Varnau, V.; O'Konek, J. J.; Choi, S. K. Reactivity and mechanism of α-nucleophile scaffolds as catalytic organophosphate scavengers. *Org. Biomol. Chem.* **2019**, *17*, 3951−3963.
(47) Latypov, S. K.; Polyancev, F. M.; Yakhvarov, D. G.; Sinyashin, O. G. Quantum chemical calculations of 31P NMR chemical shifts: scopes and limitations. *Phys. Chem. Chem. Phys.* **2015**, *17*, 6976−6987.
(48) Wilson, C.; Cooper, N. J.; Briggs, M. E.; Cooper, A. I.; Adams, D. J. Investigating the breakdown of the nerve agent simulant methyl paraoxon and chemical warfare agents GB and VX using nitrogen containing bases. *Org. Biomol. Chem.* **2018**, *16*, 9285−9291.
(49) Moser, A.; Range, K.; York, D. M. Accurate Proton Affinity and Gas-Phase Basicity Values for Molecules Important in Biocatalysis. *J. Phys. Chem. B* **2010**, *114*, 13911−13921.
(50) Iché-Tarrat, N.; Barthelat, J.-C.; Rinaldi, D.; Vigroux, A. Theoretical Studies of the Hydroxide-Catalyzed P−O Cleavage Reactions of Neutral Phosphate Triesters and Diesters in Aqueous Solution: Examination of the Changes Induced by H/Me Substitution. *J. Phys. Chem. B* **2005**, *109*, 22570−22580.
(51) Zheng, F.; Zhan, C.-G.; Ornstein, R. L. Theoretical studies of reaction pathways and energy barriers for alkaline hydrolysis of phosphotriesterase substrates paraoxon and related toxic phosphofluoridate nerve agents. *J. Chem. Soc., Perkin Trans. 2* **2001**, 2355−2363.
(52) Reddy, V. P.; Aryal, P.; Darkwah, E. K. Advanced Glycation End Products in Health and Disease. *Microorganisms* **2022**, *10*, No. 1848.
(53) Frisch, M. J.; Trucks, G. W.; Schlegel, H. B.; Scuseria, G. E.; Robb, M. A.; Cheeseman, J. R.; Scalmani, G.; Barone, V.; Petersson, G. A.; Nakatsuji, H.; Li, X.; Caricato, M.; Marenich, A. V.; Bloino, J.; Janesko, B. G.; Gomperts, R.; Mennucci, B.; Hratchian, H. P.; Ortiz, J. V.; Izmaylov, A. F.; Sonnenberg, J. L.; Williams-Young, D.; Ding, F.; Lipparini, F.; Egidi, F.; Goings, J.; Peng, B.; Petrone, A.; Henderson, T.; Ranasinghe, D.; Zakrzewski, V. G.; Gao, J.; Rega, N.; Zheng, G.; Liang, W.; Hada, M.; Ehara, M.; Toyota, K.; Fukuda, R.; Hasegawa, J.; Ishida,

https://doi.org/10.1021/acsomega.4c09946
ACS Omega 2025, 10, 12294−12305

M.; Nakajima, T.; Honda, Y.; Kitao, O.; Nakai, H.; Vreven, T.; Throssell, K.; Montgomery, J. A.; Peralta, J. E.; Ogliaro, F.; Bearpark, M. J.; Heyd, J. J.; Brothers, E. N.; Kudin, K. N.; Staroverov, V. N.; Keith, T. A.; Kobayashi, R.; Normand, J.; Raghavachari, K.; Rendell, A. P.; Burant, J. C.; Iyengar, S. S.; Tomasi, J.; Cossi, M.; Millam, J. M.; Klene, M.; Adamo, C.; Cammi, R.; Ochterski, J. W.; Martin, R. L.; Morokuma, K.; Farkas, O.; Foresman, J. B.; Fox, D. J. *Gaussian 16*, Revision C.01; Gaussian, Inc.: Wallingford CT, 2019.

(54) Grimme, S.; Hansen, A.; Brandenburg, J. G.; Bannwarth, C. Dispersion-Corrected Mean-Field Electronic Structure Methods. *Chem. Rev.* **2016**, *116*, 5105−5154.

(55) Wong, P. T.; Bhattacharjee, S.; Cannon, J.; Tang, S.; Yang, K.; Bowden, S.; Varnau, V.; O'Konek, J. J.; Choi, S. K. Reactivity and Mechanism of α-Nucleophile Scaffolds as Catalytic Organophosphate Scavengers. *Org. Biomol. Chem.* **2019**, *17* (16), 3951−3963.

(56) Bochevarov, A. D.; Harder, E.; Hughes, T. F.; Greenwood, J. R.; Braden, D. A.; Philipp, D. M.; Rinaldo, D.; Halls, M. D.; Zhang, J.; Friesner, R. A. Jaguar: A High-performance Quantum Chemistry Software Program with Strengths in Life and Materials Sciences. *Int. J. Quantum Chem.* **2013**, *113* (18), 2110−2142.

(57) Takano, Y.; Houk, K. N. Benchmarking the Conductor-like Polarizable Continuum Model (CPCM) for Aqueous Solvation Free Energies of Neutral and Ionic Organic Molecules. *J. Chem. Theory Comput.* **2005**, *1* (1), 70−77.

(58) Wertz, D. H. Relationship between the Gas-Phase Entropies of Molecules and Their Entropies of Solvation in Water and 1-Octanol. *J. Am. Chem. Soc.* **1980**, *102* (16), 5316−5322.

https://doi.org/10.1021/acsomega.4c09946
ACS Omega 2025, 10, 12294−12305